

PREDICTING THE EFFECT OF COMPRESSIBILITY IN WALL-BOUNDED TURBULENCE USING RESOLVENT ANALYSIS

Scott T. M. Dawson

Mechanical, Materials and Aerospace Engineering Department
Illinois Institute of Technology
Chicago, Illinois, 60616 USA
sdawson5@iit.edu

Beverley J. McKeon

Graduate Aerospace Laboratories
California Institute of Technology
Pasadena, California, 91125 USA
mckeon@caltech.edu

ABSTRACT

This work applies resolvent analysis to compressible zero-pressure-gradient turbulent boundary layers, for freestream Mach numbers up to 4. We investigate the effects of compressibility on predicted flow structures, and, in particular, look at how such effects may be attributed to changes in mean properties. By leveraging the similarity between the compressible and incompressible resolvent operators, as well as the Strong Reynolds Analogy, we show that the shape of the streamwise velocity and temperature components of resolvent response modes in the compressible regime can be approximated using ideas from wavepacket pseudospectral theory. This gives a means of predicting the shape of resolvent mode components for compressible flows without requiring the singular value decompositions of discretised operators. These approximations give accurate prediction of mode shapes for a Mach number of 2, but lose some quantitative accuracy at higher Mach numbers.

INTRODUCTION

Understanding the nature of high-speed wall-bounded turbulent flows is of interest for a variety of aerodynamic applications. For sufficiently high flow velocity, compressibility effects can play a significant role in the properties of boundary layers, affecting both skin friction and heat transfer. Such effects are important for the efficient and reliable flight of hypersonic vehicles.

At low to moderate Mach numbers, much of the effect of compressibility can be accounted for by changes in the mean properties of the state variables (Morkovin, 1962; Van Driest, 1951; Spina *et al.*, 1994). In particular, Morkovin's hypothesis (Morkovin, 1962) that the dynamics of compressible flows are similar to the incompressible case, and the Strong Reynolds Analogy (also due to Morkovin) relating velocity and temperature fluctuations, and its extensions (Gaviglio, 1987; Zhang *et al.*, 2014), suggest that methods that have been successful in explaining and predicting features of incompressible flows might have similar success in

the compressible regime.

For incompressible flows, the singular value decomposition of the resolvent operator corresponding to a specified spatiotemporal wavenumber has proven to be valuable for predicting and understanding wall-bounded turbulence (McKeon & Sharma, 2010; McKeon, 2017). In the compressible regime, the stability of laminar compressible boundary layers has been the subject of a number of studies (Lees & Lin, 1946; Malik, 1990; Hanifi *et al.*, 1996; Özgen & Kircali, 2008). However, there has been less work applying operator based decompositions to fully-developed compressible turbulent boundary layers (though compressible jet flows have received some attention, e.g., Jeun *et al.* (2016); Towne *et al.* (2018); Rigas *et al.* (2017)).

The present study extends the analyses utilising resolvent analysis to study compressibility effects in high-speed turbulent boundary layers. In particular, we focus on the comparison of mode shapes and amplification factors computed from resolvent analysis of the compressible and incompressible Navier-Stokes equations. The mean data for these analyses are taken from direct numerical simulations of the compressible system (Pirozzoli & Bernardini, 2011). We also explore how analytic approximations of the leading response mode shapes (as in (Dawson & McKeon, 2019a) for the incompressible case) may be applied to predict the shape of compressible resolvent response modes, providing both computational benefits and a theoretical understanding of observed structures.

GOVERNING EQUATIONS AND METHOD Resolvent formulation

In this paper, we consider both the compressible and incompressible Navier-Stokes equations. Applying Fourier transformations in the streamwise and spanwise directions and in time, these equations may be expressed symbolically as

$$(-i\omega I + L_i)\mathbf{q}_i = \mathbf{f}_i, \quad (-i\omega I + L_c)\mathbf{q}_c = \mathbf{f}_c, \quad (1)$$

where the subscripts i and c refer to the incompressible and compressible cases, respectively. The state variables for each case are given by $\mathbf{q}_i = (u, v, w, P)$ and $\mathbf{q}_c = (u, v, w, \rho, T)$, where (u, v, w) are the Fourier-transformed, mean-subtracted velocity components in the streamwise, wall-normal and spanwise directions, and P, ρ , and T are the Fourier-transformed, mean-subtracted pressure, density, and temperature. The operators L_i and L_c represent the Navier-Stokes equations for incompressible and compressible flow linearised about the corresponding mean profiles for each variable, which are assumed to be known. The right-hand-side terms of equation 1, \mathbf{f}_i and \mathbf{f}_c , represent the remaining nonlinear terms of the incompressible and compressible Navier-Stokes equations. We will additionally consider the incompressible operator linearized about the compressible mean, which we denote by $L_{i,c}$.

For the compressible Navier-Stokes equations, we assume a perfect gas with constant specific heat coefficients and constant Prandtl number, with viscosity varying with temperature according to the standard Sutherland relationship. The resolvent forcing and response modes for a given set of spatiotemporal wavenumbers are given by taking the singular value decomposition of the resolvent operators

$$\mathcal{H}_i = (-i\omega I + L_i)^{-1}, \quad (2)$$

$$\mathcal{H}_c = (-i\omega I + L_c)^{-1}, \quad (3)$$

$$\mathcal{H}_{i,c} = (-i\omega I + L_{i,c})^{-1}. \quad (4)$$

The leading right and left singular vectors of the resolvent operator give the leading forcing and response modes, which we denote by ϕ_1 and ψ_1 respectively. These are associated with a corresponding gain (i.e., the amount by which the resolvent operator amplifies the optimal forcing while mapping to the optimal response) given by the leading singular value, σ_1 . For the most part, we assume a standard kinetic energy norm for the incompressible case, and a norm that eliminates pressure-related work for the compressible case (Chu, 1965; Mack, 1984). Further details about the resolvent formulation for compressible wall-bounded flows is given in Dawson & McKeon (2019b).

We discretise in the wall-normal direction using a Chebyshev collocation method, on a grid which is transformed by a rational transformation to increase resolution near the wall, and decrease resolution in the far-field (Schmid & Henningson, 2012).

Mean data for compressible boundary layer is obtained from the publicly available data associated with the work of Pirozzoli & Bernardini (2011), while additional incompressible data is obtained from the numerical simulations of Wu *et al.* (2017).

Mode shape prediction

In recent work (Dawson & McKeon, 2019a), we have shown that, subject to certain conditions, resolvent response mode shapes for incompressible wall-bounded flows may be approximated analytically, by using ideas from wavepacket pseudospectral theory (Trefethen, 2005). Note that similar ideas have been used in other contexts in fluid mechanics in Obrist & Schmid (2010), Edstrand *et al.* (2018), and Mao & Sherwin (2011).

To make the application of wavepacket pseudospectral theory tractable, rather than considering the Navier-Stokes equations directly, we start with a decomposition

of the resolvent operator into Orr-Sommerfeld and Squire components (Rosenberg & McKeon, 2019), and utilise the fact that the amplification is dominated by the action of the Orr-Sommerfeld component, through the lift-up mechanism. This allows us to instead consider a scalar operator, which can be further simplified to give

$$L_a = ik_x U'(y_c)(y - y_c) - (Re)^{-1} \Delta. \quad (5)$$

Here Re is the Reynolds number, Δ is the Laplacian operator, and the mean streamwise velocity profile $U(y)$ has been linearized about the critical layer location, y_c (the wall-normal height where the wavespeed $c = \omega/k_x$ is equal to the mean streamwise velocity). With the selection of an appropriate norm, the resolvent response modes associated with the operator in equation 5 closely match those for the streamwise velocity (and wall-normal vorticity) for the full incompressible Navier-Stokes system. Furthermore, wavepacket pseudospectral theory suggests that in certain regimes, components of leading resolvent response modes for this scalar operator should resemble wavepackets of the form

$$\psi_a(y) = C \exp \left[a(y - y_c) - b(y - y_c)^2 \right], \quad (6)$$

where $b > 0$, and the constant C is defined such that the mode has unit norm. With this assumed mode shape, approximating resolvent response mode amounts to finding the parameters a and b that maximizes the resolvent response, or equivalently minimizes

$$J(a, b) = \|(-i\omega I + L_a)\psi_a(y)\|^2. \quad (7)$$

After substituting in the template mode shape given in equation 5, the minimiser of the cost function in equation 7 may be found from computing the roots of a polynomial equation. As well as giving a theoretical explanation for observed mode shapes, this analysis precludes the need for numerical singular value decomposition, potentially giving a substantial reduction in computational cost. This work will study how these methods, described in more detail in Dawson & McKeon (2019a), may be applied to predict the shape of components of resolvent response modes for compressible flows.

RESULTS

Resolvent mode shape and amplification

Here we present sample results from resolvent analysis of a compressible boundary layer. We will focus on spatial wavenumbers $k_x = \pi/9$ and $k_z = 2\pi/3$ (where x indicates the streamwise direction, and z the spanwise direction), which correspond to the typical size of very large scale motions (VLSM).

Figure 1 shows the leading two singular values for these wavenumbers, as a function of the wavespeed c , as well as the eigenvalues of the compressible linear operator, L_c , with Mach number $M = 2$ and friction Reynolds number $Re_\tau = 900$. Singular values of \mathcal{H}_c are shown for the compressible resolvent operator with both the standard compressible norm, and for a seminorm that only weights

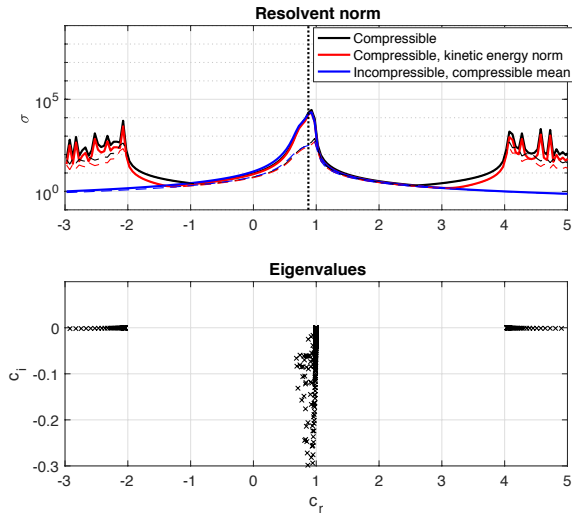


Figure 1. Leading two resolvent singular values (top, solid lines for σ_1 , dashed lines for σ_2) and eigenvalues (bottom) for compressible boundary layer flow with Mach number $M = 2$, $Re_\tau = 900$, and spatial wavenumbers $k_x = \pi/9$, $k_z = 2\pi/3$. Singular values are also shown for $\mathcal{H}_{i,c}$, the incompressible operator linearised about the compressible mean. The vertical dotted line represents the wavespeed ($c = 0.875$) chosen for subsequent analysis in this paper.

the velocity components (and thus can be considered to be a kinetic energy norm). Also shown are the singular values of $\mathcal{H}_{i,c}$, the incompressible resolvent operator linearised about the compressible mean velocity profile. We observe that for all cases, there is high amplification for wavespeeds $c \approx 0.8 - 0.9$ (normalized by the freestream velocity), which is typical of VLSM. This region also shows a relatively large spectral gap between σ_1 and σ_2 for all cases, suggesting that the leading set of forcing and response modes captures a substantial component of the amplification of the resolvent operators within this regime. At much larger and smaller wavespeeds, we observe substantial differences between the incompressible and compressible operators, owing to the presence of acoustic eigenmodes with close to neutral stability, which are only present for compressible operators. Note that the location of these acoustic modes varies with the choice of spatial wavenumber. We lastly observe that the choice of norm makes little difference in the qualitative behavior of the singular values of the compressible resolvent operator.

Figure 2 shows the shape of the leading resolvent forcing and response modes for each of the resolvent operators considered in figure 1, as well as the incompressible operator using an incompressible mean, all computed at a wavespeed $c = 0.875$. For the incompressible operators, the temperature field is obtained by appending a scalar transport equation to the incompressible Navier-Stokes equations, as described in Dawson *et al.* (2018) and Saxton-Fox (2018). Note that the incompressible operators do not have a fluctuating density field, and that the cases with a kinetic energy norm do not have forcing components in the thermodynamic variables. Aside from these caveats, we observe very little variation in the resolvent forcing and response amplitudes, both in terms of the shape and relative ampli-

tude of each variable. The largest difference is in the location of the peak for the incompressible operator with incompressible mean velocity field, which can be attributed to a shift in the critical layer location for this wavespeed. Figure 3 shows two-dimensional contours of these modes at a given spanwise location for \mathcal{H}_c and \mathcal{H}_i . This shows that the phase behavior is also similar for both the compressible and incompressible cases, with inclined structures observed for the temperature, and streamwise and spanwise velocity fields, and very little phase variation in the wall-normal velocity with distance from the wall. This suggests that in this regime, the leading amplification mechanisms for the compressible resolvent operator strongly resemble those for the incompressible case.

Mode shape prediction

It was observed in figure 2 that the largest components of the leading resolvent response modes are the streamwise velocity and temperature fields. This observation, and the similarity between the shapes of the streamwise velocity and temperature mode components observed in figure 3, suggests that these fields are both amplified by a single mechanism. Furthermore, the similarity between the leading response modes of \mathcal{H}_c and $\mathcal{H}_{i,c}$ suggests that this mechanism is closely related to that which dominates the response for incompressible flows. This suggests that methods to predict these mode shapes that have been successful in the incompressible regime might be readily extend for compressible flows.

Figure 4 compares the streamwise velocity component of several numerically computed resolvent response modes of \mathcal{H}_c and $\mathcal{H}_{i,c}$, with those predicted by solving the appropriately defined optimisation problem given in equation 7 to find predicted wavepacket shape parameters. We observe that this method accurately predicts both the mode amplitude and phase variation near the critical layer, with the accuracy improving for larger spatial wavenumbers. This can be explained, at least in part, by the fact that the mode shape approximation relies upon a linearisation of the mean velocity profile about the critical layer, which will be more accurate for modes that are concentrated around the critical layer. Figure 5 shows that this approach can also be used to predict the shape of temperature modes, which is perhaps unsurprising due to their close resemblance to streamwise velocity modes (with some differences attributable to the nonunitary Prandtl number), as is consistent with the Strong Reynolds Analogy (Morkovin, 1962; Smits & Dussauge, 2006).

Effect of Mach number

So far, we have only considered compressible flows with a freestream Mach number of 2, where we have found that the behavior of resolvent modes are similarly predicted for the incompressible and compressible operator. Figure 6 shows that this approximation becomes less accurate as the Mach number increases to 3 and 4. As a consequence, the mode shape prediction (which is developed using incompressible operators with compressible means) also becomes less accurate with increasing Mach number. However, the resolvent modes considered here still retain the same qualitative features as the Mach number is increased.

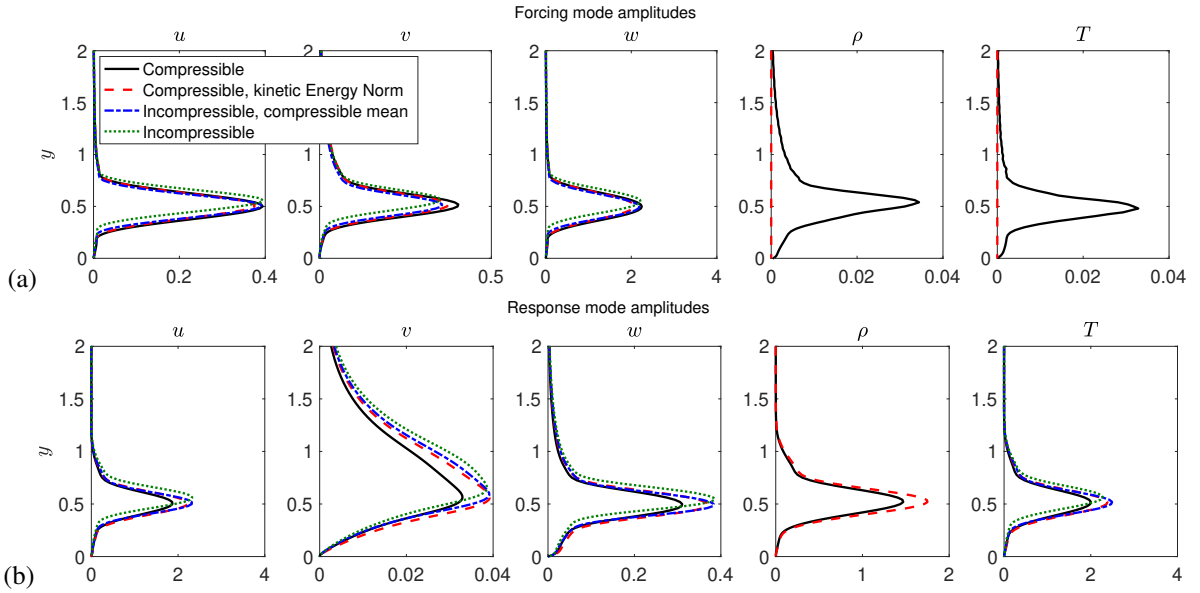


Figure 2. Components of leading resolvent (a) forcing and (b) response modes for various incompressible and compressible ($M = 2$) resolvent operators, with friction Reynolds number $Re_\tau = 900$, spatial wavenumbers $k_x = \pi/9$, $k_z = 2\pi/3$ and wavespeed $c = 0.875$.

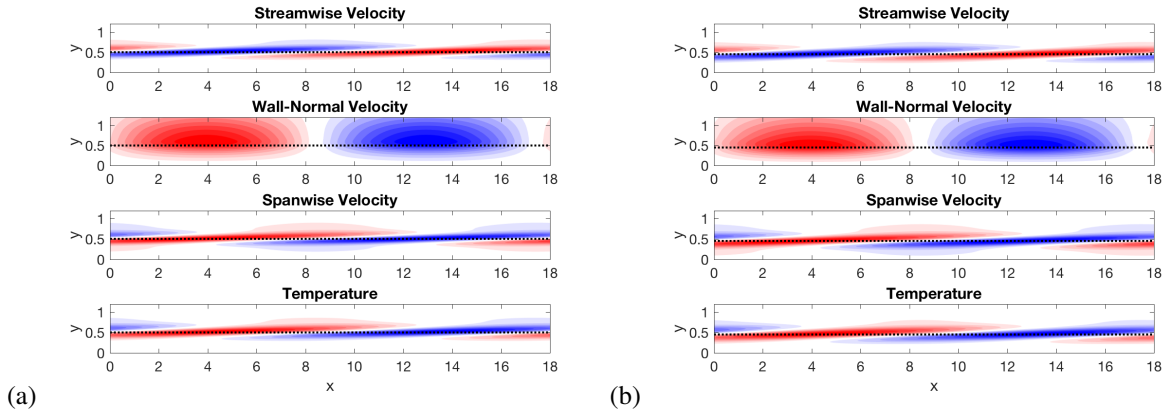


Figure 3. Leading resolvent mode shapes through a cross-section at a given spanwise location, for (a) incompressible and (b) compressible ($M = 2$) flow, with parameters the same as those plotted in figure 2. Red and blue contours represent positive and negative values of mean-subtracted variables, while the dashed black line represents the location of the critical layer.

CONCLUSIONS

We have demonstrated that resolvent analysis of compressible zero-pressure-gradient turbulent boundary layer flows gives modes shapes similar to the incompressible case when using spatiotemporal wavenumbers typical of very large scale motions. In particular, the incompressible resolvent operator linearised about a compressible mean profile produces very similar mode shapes and amplification levels to the compressible operator, which can be viewed as a successful demonstration of the Morkovin hypothesis (Morkovin, 1962). This similarity with the incompressible case allows for the application of techniques developed for the incompressible equations, such as the prediction of the shape of components of the modes. As well as showing that mode shape predictions can be applied to approximate the streamwise velocity component of compressible boundary layers, we also have shown that a similar approach can approximate the shape of the temperature field, as is consistent with the Strong Reynolds Analogy. These methods are particularly successful up to a Mach number of 2, with larger

deviations between the results found at higher Mach numbers. The scaling of these results with Mach number, and comparison with observed variations in turbulent structures with increasing Mach number (Smits *et al.*, 1989; Duan *et al.*, 2011) is the subject of ongoing work.

ACKNOWLEDGEMENTS

The authors gratefully acknowledge H. Jane Bae for insightful comments and suggestions on a draft of this manuscript.

REFERENCES

- Chu, B.-T. 1965 On the energy transfer to small disturbances in fluid flow (part i). *Acta Mechanica* **1** (3), 215–234.
- Dawson, S. T. M. & McKeon, B. J. 2019a On the shape of resolvent modes in wall-bounded turbulence. *arXiv preprint arXiv:1901.10913*.

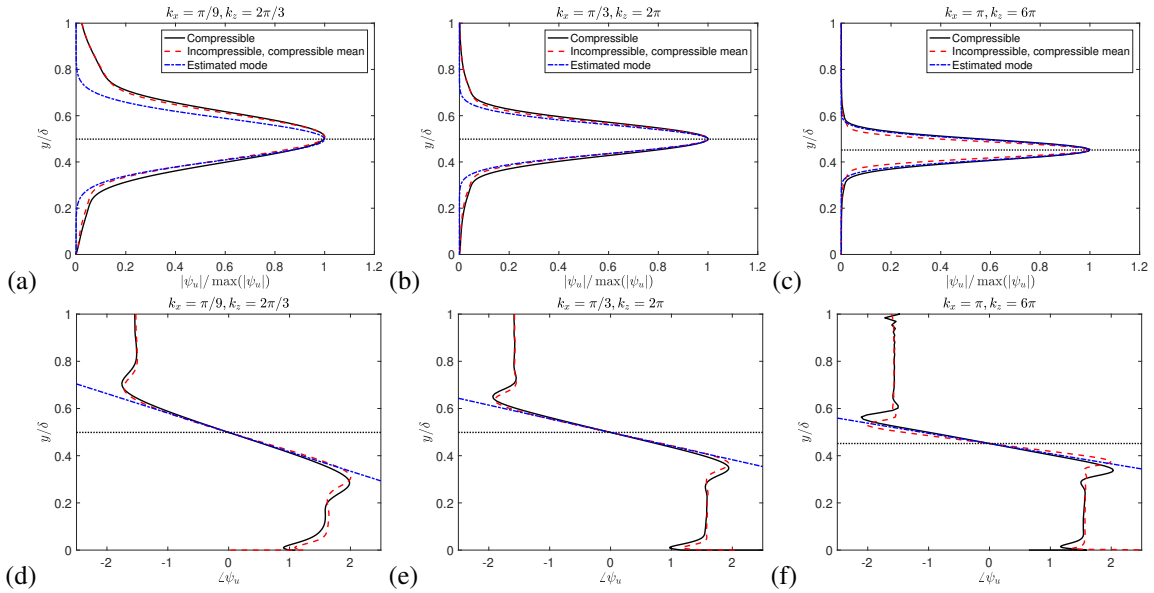


Figure 4. Comparison between streamwise velocity mode amplitudes (a-c) and phases (d-f) for numerically computed modes using the compressible ($M = 2$) and incompressible resolvent operators (with compressible mean data), and predicted mode shapes found from optimising equation 7. Subplots (a,d) use the same wavenumbers as figure 2, while (b,d) and (c,e) consider streamwise and spanwise wavenumbers that are 3 and 9 times larger, respectively. The horizontal dotted line denotes the location of the critical layer.

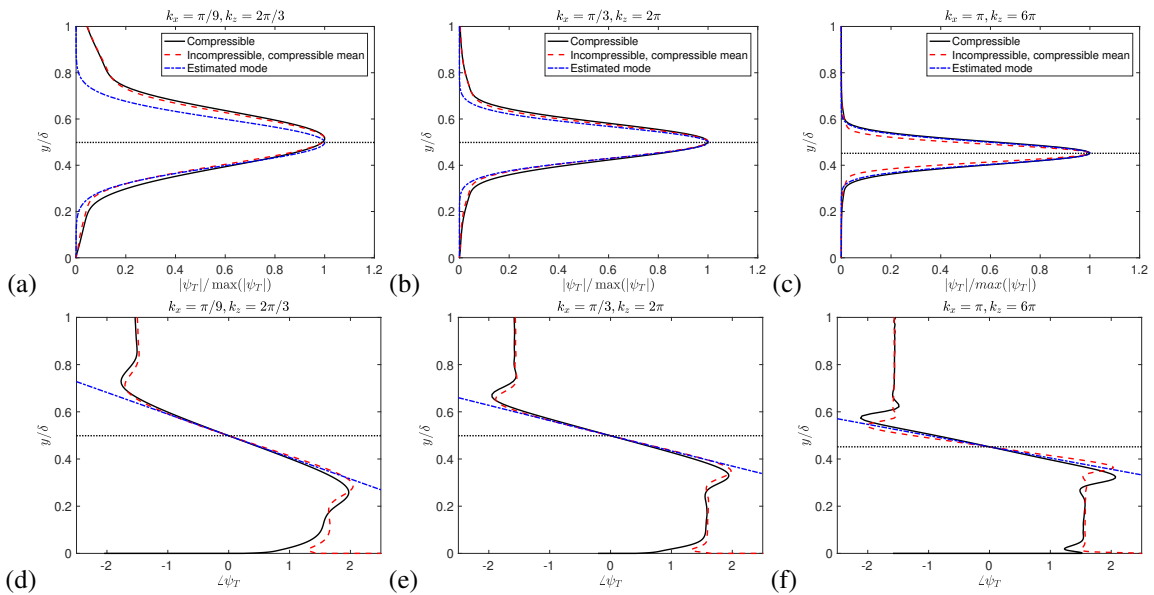


Figure 5. As for figure 4, but considering the temperature rather than streamwise velocity.

Dawson, S. T. M. & McKeon, B. J. 2019b Studying the effects of compressibility in planar Couette flow using resolvent analysis. In *AIAA Scitech 2019 Forum*, p. 2139.

Dawson, S. T. M., Saxton-Fox, T. & McKeon, B. J. 2018 Modeling passive scalar dynamics in wall-bounded turbulence using resolvent analysis. In *2018 Fluid Dynamics Conference*, p. 4042.

Duan, L., Beekman, I. & Martín, M. P. 2011 Direct numerical simulation of hypersonic turbulent boundary layers. Part 3. effect of Mach number. *Journal of Fluid Mechanics* **672**, 245–267.

Edstrand, A. M., Schmid, P. J., Taira, K. & Cattafesta, L. N. 2018 A parallel stability analysis of a trailing vortex wake. *Journal of Fluid Mechanics* **837**, 858–895.

Gaviglio, J. 1987 Reynolds analogies and experimental

study of heat transfer in the supersonic boundary layer. *International journal of heat and mass transfer* **30** (5), 911–926.

Hanifi, A., Schmid, P. J. & Henningson, D. S. 1996 Transient growth in compressible boundary layer flow. *Physics of Fluids* **8** (3), 826–837.

Jeun, J., Nichols, J. W. & Jovanović, M. R. 2016 Input-output analysis of high-speed axisymmetric isothermal jet noise. *Phys. Fluids* **28** (4), 047101.

Lees, L. & Lin, C. C. 1946 Investigation of the stability of the laminar boundary layer. *Tech. Rep.* 1115. NACA.

Mack, L. M. 1984 Boundary-layer linear stability theory. *Tech. Rep.* 709. AGARD.

Malik, M. R. 1990 Numerical methods for hypersonic boundary layer stability. *Journal of Computational*

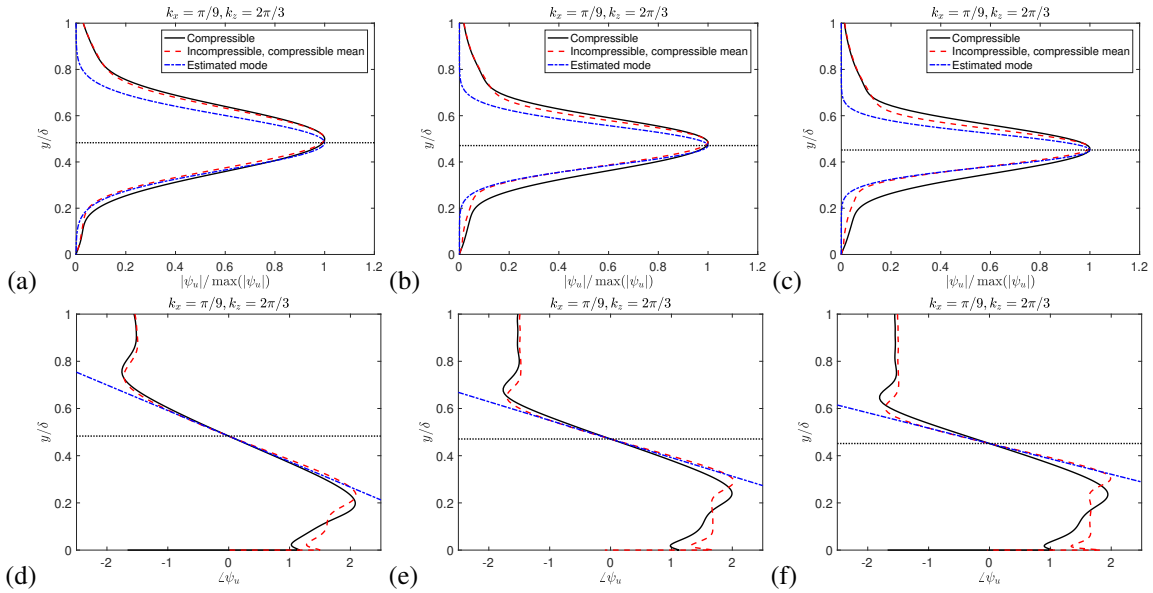


Figure 6. Comparison between streamwise velocity mode amplitudes (a-c) and phases (d-f) for numerically computed modes using the compressible and incompressible resolvent operators (with compressible mean data), and predicted mode shapes found from optimising equation 7. Spatial wavenumbers are the same as those in figure 2, with Mach numbers of 2 (a,d), 3 (b,e) and 4 (c,f) and Reynolds numbers $Re_\tau = 450$ (a,d) and 500 (b,c,e,f).

Physics **86** (2), 376–413.

Mao, X. & Sherwin, S. J. 2011 Continuous spectra of the batchelor vortex. *Journal of Fluid Mechanics* **681**, 1–23.

McKeon, B. J. 2017 The engine behind (wall) turbulence: perspectives on scale interactions. *Journal of Fluid Mechanics* **817**, P1.

McKeon, B. J. & Sharma, A. S. 2010 A critical-layer framework for turbulent pipe flow. *Journal of Fluid Mechanics* **658**, 336–382.

Morkovin, M. V. 1962 Effects of compressibility on turbulent flows. *Mécanique de la Turbulence* **367**, 380.

Obrist, D. & Schmid, P. J. 2010 Algebraically decaying modes and wave packet pseudo-modes in swept Hiemenz flow. *Journal of Fluid Mechanics* **643**, 309–332.

Özgen, S. & Kircali, S. A. 2008 Linear stability analysis in compressible, flat-plate boundary-layers. *Theoretical and Computational Fluid Dynamics* **22** (1), 1–20.

Pirozzoli, S. & Bernardini, M. 2011 Turbulence in supersonic boundary layers at moderate Reynolds number. *Journal of Fluid Mechanics* **688**, 120–168.

Rigas, G., Schmidt, O. T., Colonius, T. & Bres, G. A. 2017 One way Navier-Stokes and resolvent analysis for modeling coherent structures in a supersonic turbulent jet. In *23rd AIAA/CEAS Aeroacoustics Conference*, p. 4046.

Rosenberg, K. & McKeon, B. J. 2019 Efficient representation of exact coherent states of the Navier–Stokes equations using resolvent analysis. *Fluid Dynamics Research* **51**, 011401.

Saxton-Fox, T. 2018 Coherent structures, their interactions, and their effects on passive scalar transport and aerodynamic distortion in a turbulent boundary layer. PhD thesis, California Institute of Technology.

Schmid, P. J. & Henningson, D. S. 2012 *Stability and transition in shear flows*. Springer Science & Business Media.

Smits, A. J. & Dussauge, J.-P. 2006 *Turbulent shear layers in supersonic flow*. Springer Science & Business Media.

Smits, A. J., Spina, E. F., Alving, A. E., Smith, R. W., Fernando, E. M. & Donovan, J. F. 1989 A comparison of the turbulence structure of subsonic and supersonic boundary layers. *Physics of Fluids A: Fluid Dynamics* **1** (11), 1865–1875.

Spina, Eric F, Smits, Alexander J & Robinson, Stephen K 1994 The physics of supersonic turbulent boundary layers. *Annual Review of Fluid Mechanics* **26** (1), 287–319.

Towne, A., Schmidt, O. T. & Colonius, T. 2018 Spectral proper orthogonal decomposition and its relationship to dynamic mode decomposition and resolvent analysis. *Journal of Fluid Mechanics* **847**, 821–867.

Trefethen, L. N. 2005 Wave packet pseudomodes of variable coefficient differential operators. In *Proceedings of the Royal Society of London A: Mathematical, Physical and Engineering Sciences*, vol. 461, pp. 3099–3122. The Royal Society.

Van Driest, E. R. 1951 Turbulent boundary layer in compressible fluids. *Journal of the Aeronautical Sciences* **18** (3), 145–160.

Wu, X., Moin, P., Wallace, J. M., Skarda, J., Lozano-Durán, A. & Hickey, J.-P. 2017 Transitional–turbulent spots and turbulent–turbulent spots in boundary layers. *Proceedings of the National Academy of Sciences* pp. E5292–E5299.

Zhang, Y.-S., Bi, W.-T., Hussain, F. & She, Z.-S. 2014 A generalized reynolds analogy for compressible wall-bounded turbulent flows. *Journal of Fluid Mechanics* **739**, 392–420.